CHUKHOVSKII, F. N., GABRIELYAN, K. T. & PETRASHEN', P. V. (1976). *Proc. IV Conf. on the Dynamical Effects of the Scattering of X-rays and Electrons*, Leningrad, pp. 17–20. (In Russian.)

CHUKHOVSKII, F. N. & PETRASHEN', P. V. (1977). *Acta Cryst.* A**33**, 311–319.

COURANT, R. (1962). *Partial Differential Equations*. New York/London: Interscience.

ERDELYI, A. (1953). *Higher Transcendental Functions*. Vol. I. New York: McGraw-Hill.

FUKUHARA, A.. & TAKANO, Y. (1977). *Acta Cryst.* A**33**, 137–142.

KATAGAWA, T. & KATO, N. (1974). *Acta Cryst.* A**30**, 830–836.

MILLER, J. C. P. (1955). *Tables of Weber Parabolic Cylinder Functions*. London: Her Majesty's Stationery Office.

PENNING, P. & POLDER, D. (1961). *Philips Res. Rep.* **16**, 419–440.

PETRASHEN', P. V. (1973). *Fiz. Tverd. Tela*, **15**, 3131–3132.

PETRASHEN', P. V. & CHUKHOVSKII, F. N. (1975). *Zh. Eksp. Teor. Fiz.* **69**, 477–487.

PETRASHEN', P. V. & CHUKHOVSKII, F. N. (1976). *Kristallografiya*, **21**, 283–292.

PINSKER, Z. G. (1974). *The X-ray Dynamical Scattering by Perfect Crystals*. Moscow: Nauka. (In Russian.)

SMIRNOV, V. I. (1958). *Course of Higher Mathematics*, Vol. IV, pp. 795–806. Moscow: GIPML. (In Russian.)

TAUPIN, D. (1964). *Bull. Soc. Fr. Minéral. Cristallogr.* **87**, 469–514.

Acta Cryst. (1978). A**34**, 621–625

A Simple Refinement of Density Distributions of Bonding Electrons. III. Experimental Static Electron Densities for the Diborane Molecule

BY C. SCHERINGER, D. MULLEN AND E. HELLNER

Institut für Mineralogie der Universität Marburg, D-3550 Marburg, Federal Republic of Germany

(*Received* 26 *August* 1977; *accepted* 14 *March* 1978)

From recently refined models of the electron density distribution in the diborane molecule, static density sections are calculated and presented as difference densities ρ(molecule at rest) $-$ ρ(isolated atoms at rest). The sections obtained are compared with corresponding ones derived from quantum-chemical calculations by Laws, Stevens and Lipscomb.

Introduction

In a preceding paper we described the refinement of two models of the electron density distribution in the diborane molecule (Mullen & Hellner, 1977), where the X-ray data, collected at 90 K, of Smith & Lipscomb (1965) were used. In this paper we shall compare the results of our refinement with the results of quantum-chemical calculations. For diborane, two SCF calculations were carried out by Laws, Stevens & Lipscomb (1972) (LSL), one with a minimum basis of 18 Slater-type orbitals (STO's), and one with an expanded basis of 68 STO's. Since the quantum-chemical calculations of LSL were performed for the static density of the equilibrium configuration of the molecule, we have transformed our experimentally obtained, dynamic densities (*i.e.* densities including the effects of the thermal motions of the atoms) into static densities.

Thermal deconvolution and series termination

Deconvolution of the dynamic densities for thermal smearing can be exactly performed (in the convolution approximation), if the temperature factors for all density units of the model are known. In actual practice we can assume this if the temperature factors were determined with the highest possible accuracy of the present-day methods (see below). However, the static density distribution, obtained by Fourier synthesis with structure factors, is disturbed by series-termination errors. The peaks that can be observed in difference density maps are broadened and reduced in height (Scheringer, 1977*a*). We cannot overcome the effect of series termination since the measured data are always limited, and thus we cannot reconstruct the true density distribution in the molecule, although we could reconstruct a more accurate representation of the refined density model.*

* Since the structure factors are calculated from a static density model, it is possible to calculate more structure factors than correspond to the experimental limit of $(\sin\theta)/\lambda$. With such a set of structure factors a higher degree of resolution would be suggested than is actually given by the diffraction experiment. Certain (large gradient) details in the static density maps would then be artifacts. Therefore the series should be terminated at the experimental limit of $(\sin\theta)/\lambda$ (Dietrich & Scheringer, 1978).

Thus, the appropriate counterpart of an experimental static density is a quantum-chemically calculated density distribution treated with the series termination as given by the experimental data. The series-termination effect evens out all large density gradients, such as the nuclear cusps, of the theoretical model. Since the quantum-chemically calculated difference maps published are usually not treated with series termination, we can only make an estimate of the true heights of bond and lone-pair electron peaks where these peaks can be recognized in the experimental static maps (Scheringer, 1977*a*). But we emphasize that a further comparison of theoretical and experimental static maps beyond the resolution limit (set by the experimental data) is meaningless and hence should not be made.

Since the temperature factors can be determined with a reasonable accuracy from a limited set of experimental data (or from neutron data) the crucial factor that impairs the comparison of experimental and theoretical maps is the series-termination effect. In view of this, there is no need to design models for the least-squares refinement with X-ray data that have the complexity (large density gradients) of quantum-chemical models. This justifies the use of the coarser empirical models that have been used in the X-ray analysis of density distributions (Hirshfeld, 1971; Brill, Dietrich & Dierks, 1971; Dietrich & Scheringer, 1978; Hellner, 1977).

We would also like to point out that there is no physical argument against the use of empirical models as long as such models achieve what they are expected to do: to supply a description of the density distribution in the molecule which can be fitted to the X-ray data. For this purpose a quantum-chemical foundation of the density model is not necessary. But we remark that the empirical model used in this work (Gaussian density distributions in the bond and lone-pair electron regions) has a quantum-chemical counterpart in the 'Gaussian lobe method' (Preuss, 1956) or the 'floating spherical Gaussian orbital method' of Frost (1977). In this context we also remark that the attempts of Coppens, Willoughby & Csonka (1971) to determine population parameters, $P_{\mu\nu}$, of the orbital products directly from the X-ray data have been discontinued, and that, in the quantum-chemical sense, 'less rigorous' models (expansion in multipoles) are being used, which satisfy the needs of structure determination much better (fewer parameters).

Since there is no neutron diffraction study for diborane, we have taken the positional and thermal parameters of the $1s^2$ orbital products, obtained in the refinement with X-ray data, as those for the nuclei (Stewart, 1970). Kutoglu & Hellner (1978) found for cyanuric acid that the positional and thermal parameters of the $1s^2$ orbital products (in the final molecular model) agreed very well with those of the neutron structure determination (Coppens & Vos, 1971). For the boron atoms in diborane the vibration tensors β_t of the $1s^2$ orbital products appear to give reasonable values for the temperature factors of the nuclei, which is confirmed by the small spread between the tensors obtained for the two models LQ1 and LQ4 respectively (Mullen & Hellner, 1977). For the hydrogen atoms the vibration tensors were also obtained from a core refinement, but the parameters are less accurate and show a greater spread for the two models. The absolute values of the vibration components are about the same for the boron and terminal hydrogen atoms, whereas the vibration components of the bridge hydrogens are smaller in the plane of the bridge and normal perpendicular to this plane, which corresponds to the stability of the bridge.

Incorrect temperature factors give rise to errors in the experimental static densities. We have estimated the errors in the vibration tensors from the spread of the tensors as found from the two different refinements with models LQ1 and LQ4 respectively. [Smith & Lipscomb's (1965) parameters were not considered here because they were derived from 86 data only.] For the boron atoms this spread is in no case more than 1% of the diagonal components of the charge-smearing tensors. For the hydrogen atoms this figure is 10%, but the average spread gives only 3·7%. A test calculation showed that an increase of 6% in all the smearing tensors of our molecular models induces a change of at most 0·07 e $Å^{-3}$ in the experimental static density for diborane. Although these results were obtained for diborane, they appear to hold quite generally, since the diagonal components of the charge-smearing tensors are always much larger than those of the vibration tensors. For other types of molecular models, where no Gaussian charge distributions are used, the interaction between vibration tensors and density parameters will be even smaller and, hence, the influence of errors in the temperature factor is likely to decrease.

Temperature factors for models which contain internuclear density units were derived in the harmonic approximation (Scheringer, 1977*b*). Although these temperature factors usually cannot exactly be calculated from the vibration tensors of the nuclei, the errors introduced into the density maps by applying simple approximations for these temperature factors are small, and are not likely to exceed 0·1 e $Å^{-3}$ (Scheringer, 1977*c*). The reason is the same as in the above discussion: the vibration tensors constitute only a small part of the smearing tensors, and thus an error in the first produces a much smaller relative error in the latter.

The procedure of calculating experimental static difference densities has a certain advantage with respect to the effect of an incorrect scale factor: since the difference density is calculated from two models (molecular minus free-atom model) on absolute scales,

this density is not directly affected by an incorrect scale factor. However, because of correlation between the scale factor and the density parameters of the molecular model, in the refinement an incorrect scale factor will falsify the density parameters to a small extent, and it is only this error which enters into the difference map.

The calculation of the experimental static densities is performed in the following steps: (1) vibration tensors for all density units in the models are identified or calculated; (2) these vibration tensors are set to zero, or are eliminated in the expression for the structure factor; (3) the Fourier synthesis of the static (difference) density is calculated with the structure factors under (2) up to the experimental limit of $(\sin\theta)/\lambda$.

We comment on the first two points. (1) For the core electrons and the lone-pair electrons the vibration tensors of the corresponding nuclei should be used. For the charge clouds between the nuclei, which represent mainly the bond charge, the vibration tensors used were calculated in an approximation which was suggested by Scheringer (1977*c*). Essentially, it consists of forming the average values of the vibration tensors of the adjacent nuclei. For the components in the direction of the bond, this average is directly used; for the components perpendicular to the bond, the average is multiplied by a factor $K < 1$. For diborane, whose X-ray data were collected at 90 K, the reduction factor proposed is $K = 0{\cdot}78$ (Scheringer, 1977*c*).

(2) In our models, the charge clouds in the lone-pair regions and in the bonds are represented by Gaussian distributions. Hence, in the structure factor, the distribution of the charge is formally treated like the temperature factor. Thus, the parameter in the refinement is a $\boldsymbol{\beta}$ tensor which simultaneously contains the smearing distribution of the charge, $\boldsymbol{\beta}_s$, and the thermal vibration, $\boldsymbol{\beta}_t$, *i.e.* $\boldsymbol{\beta}_{exp} = \boldsymbol{\beta}_s + \boldsymbol{\beta}_t$. In order to eliminate the thermal vibrations in the model, one has to put $\boldsymbol{\beta}_s = \boldsymbol{\beta}_{exp} - \boldsymbol{\beta}_t$, and use $\boldsymbol{\beta}_s$ in the structure factors.

Results

The R values obtained by Mullen & Hellner (1977) for models LQ1 and LQ4 are 0·037 and 0·026 respectively for the total set of 273 X-ray data [$(\sin\theta_{max})/\lambda = 0{\cdot}77$ Å^{-1}], measured by Smith & Lipscomb (1965) but published by Jones & Lipscomb (1970). The $F_o - F_c$ syntheses with the molecular models show that the remaining errors of the refinement are of random nature. The largest deviations from zero in these maps were $\pm 0{\cdot}1$ e Å^{-3}. The standard deviation σ for the difference maps is 0·037 e Å^{-3}, as calculated from Rees (1976), equation (10) [the remaining terms in Rees's equation (1) can be neglected for the calculation of σ]. These results indicate a reasonable quality of the data. This is also confirmed by the fact that the bond lengths increase by about 0·1 Å with the use of our two models, and thus approach the bond lengths obtained by electron diffraction (Mullen & Hellner, 1977).

The random error in the static difference density maps is difficult to obtain exactly. If we consider the random error in the difference density as a consequence of the random errors of the parameters of the model, we conclude that the random errors in dynamic and static difference densities should be about the same, since the model parameters are the same except for the temperature factors. Hence, we conclude that, to a first approximation, the estimated standard deviation in the experimental static difference density is also $\sigma = 0{\cdot}037$ e Å^{-3}.

The static difference densities ρ(molecule) − ρ(free-atom model) are given in Figs. 1 (terminal B—H bonds) and 2 (B—H—B bridges). Since the crystallographic site symmetry of the molecule is only $\bar{1}$, the maps contain each bond twice. As the molecular symmetry is *mmm*, the two sections through each bond respectively are

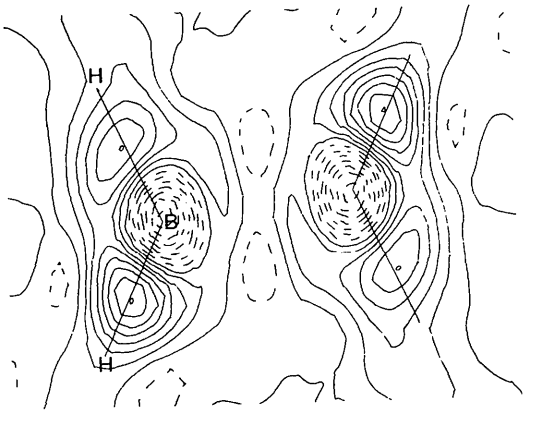

Fig. 1. Static difference density distribution in the terminal B—H bonds, ρ(molecule at rest) − ρ(free atoms at rest), obtained from Mullen & Hellner's (1977) refined model LQ1. Contour intervals are 0·05 e Å^{-3}. Zero and positive contours are solid lines, negative contours are dashed. Correction for series termination gives peak heights of approximately 0·47 and 0·36 e Å^{-3} respectively.

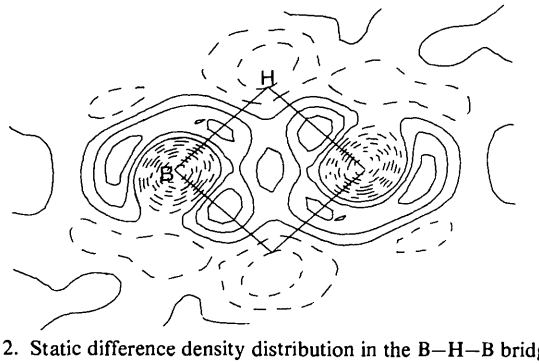

Fig. 2. Static difference density distribution in the B—H—B bridges, otherwise like Fig. 1. Correction for series termination gives peak heights of approximately 0·45 and 0·37 e Å^{-3} respectively.

chemically equivalent. Since there is no indication that the molecular symmetry is significantly disturbed by intermolecular forces of the molecules, the differences in the two chemically equivalent sections can be used to estimate the real magnitude of the errors in the maps.

For the terminal B—H bonds (Fig. 1), the peaks are located nearly in the centre of the bonds, with heights of 0·25 and 0·36 e Å^{-3} for model LQ1, and of 0·20 and 0·29 e Å^{-3} for model LQ4. Correction for series termination would indicate heights up to about 0·47 e Å^{-3}. The difference of 0·11 e Å^{-3} in the two heights corresponds to the random error, 3 σ = 0·111 e Å^{-3}. On the whole, the differences of the density distribution in the two terminal B—H bonds can be interpreted as being random, and not as being systematic.

With the B—H—B bridges, (Fig. 2) there are two separate peaks, each lying on the line B—H. The heights of the peaks are 0·11 and 0·14 e Å^{-3} for model LQ1, and 0·07 and 0·14 e Å^{-3} for model LQ4. Correction for series termination would indicate heights up to about 0·45 e Å^{-3}. Again, the differences of the density distribution in the two chemically equivalent sections can solely be attributed to random deviations.

The corrections of the peak heights for series termination were carried out by fitting a Gaussian distribution to the shape of the observed peaks (Scheringer, 1977*a*). Although this correction can only be an estimate we state that it is quite unlikely that our experimental bond peaks will be higher than 0·5 e Å^{-3}.

In order to compare our results to LSL's we have recontoured LSL's maps (LSL Fig. 5, minimum basis with 18 STO's; LSL Fig. 6, expanded basis with 68 STO's) in e Å^{-3} units, see our Figs. 3 and 4. In our maps (Figs. 1 and 2) the peaks are higher than those of LSL's minimum basis (0·33 for the terminal bond, 0·07 e Å^{-3} for the bridge, Fig. 3), and they are lower than those of LSL's expanded basis (0·74 e Å^{-3} for both bonds, Fig. 4). LSL remark that a minimum basis gives bond peaks which are too low. Hence, our peak heights are probably closer to reality than LSL's obtained with the minimum basis. On the other hand, our peaks, extrapolated for infinite resolution (0·47 and 0·45 e Å^{-3}), still remain lower than LSL's peaks calculated with the expanded basis. Furthermore, with the expanded basis, LSL's maxima are located nearly at the protons, whereas in our maps the peaks appear nearly in the middle between the B and H nuclei.

For comparison, we quote the quantum-chemical calculation for the B—H radical (Bader, Keaveny & Cade, 1967) and the X-ray investigation of decaborane (Dietrich & Scheringer, 1978). In the B—H radical the peak is 0·58 e Å^{-3} high and also located close to the proton. In decaborane, the peaks for the terminal B—H bonds, extrapolated for infinite resolution, have heights of about 0·65 e Å^{-3} but are located more towards the centre of the bonds. Hence, also in the light of the other investigations, LSL's peaks of 0·74 e Å^{-3} appear to be rather high, whereas the question of the exact location of the terminal bond peak remains open.

For both basis sets LSL find only one peak in the B—H—B bridge, which is extended towards the B—H lines. LSL comment on this with '... the two $B(H_t)_2$ units are joined primarily through hydrogen bridge bonds rather than by direct B—B linkage'. LSL do not discuss the question of a two or three-centre bond, but they find only one symmetric peak in the bridge and little density along the B—B axis. In our maps (Fig. 2) two separate peaks appear on the B—H lines, and thus also suggest the predominance of hydrogen bridge bonds. We also find little density along the B—B axis and our map would favour the absence of a three-centre bond.

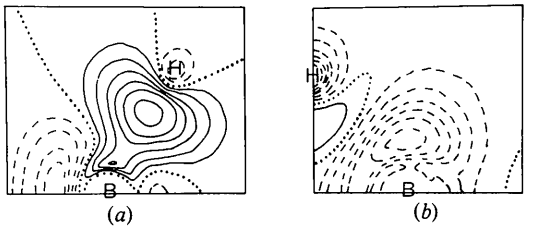

(*a*) (*b*)

Fig. 3. Difference density distribution calculated by LSL with the minimum basis (18 STO's). (*a*) terminal B—H bond. (*b*) bridge. Contours are recalculated to e Å^{-3} units. Contour intervals are 0·05 e Å^{-3}.

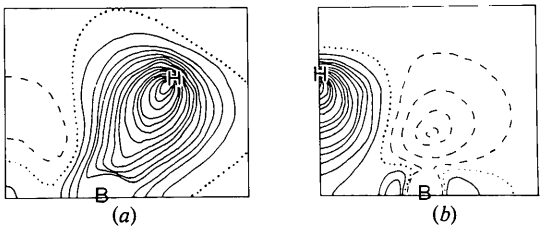

(*a*) (*b*)

Fig. 4. Difference density distribution calculated by LSL with the expanded basis (68 STO's), otherwise like Fig. 3.

References

BADER, R. F. W., KEAVENY, I. & CADE, P. E. (1967). *J. Chem. Phys.* **47**, 3381–3402.

BRILL, R., DIETRICH, H. & DIERKS, H. (1971). *Acta Cryst.* B**27**, 2003–2018.

COPPENS, P. & VOS, A. (1971). *Acta Cryst.* B**27**, 146–158.

COPPENS, P., WILLOUGHBY, T. V. & CSONKA, L. N. (1971). *Acta Cryst.* A**27**, 248–256.

DIETRICH, H. & SCHERINGER, C. (1978). *Acta Cryst.* B**34**, 54–63.

FROST, A. A. (1977). *Methods in Electronic Structure Theory*, pp. 29–49. New York and London: Plenum.

HELLNER, E. (1977). *Acta Cryst.* B**33**, 3813–3816.

HIRSHFELD, F. L. (1971). *Acta Cryst.* B**27**, 769–781.

JONES, D. S. & LIPSCOMB, W. N. (1970). *Acta Cryst.* A**26**, 196–207.

KUTOGLU, A. & HELLNER, E. (1978). *Acta Cryst.* B34, 1617–1623.
LAWS, E. A., STEVENS, R. M. & LIPSCOMB, W. N. (1972). *J. Am. Chem. Soc.* 94, 4461–4467.
MULLEN, D. & HELLNER, E. (1977). *Acta Cryst.* B33, 3816–3822.
PREUSS, H. (1956). *Z. Naturforsch. Teil A*, 11, 823–831.
REES, B. (1976). *Acta Cryst.* A32, 483–488.
SCHERINGER, C. (1977*a*). *Acta Cryst.* A33, 588–592.
SCHERINGER, C.(1977*b*). *Acta Cryst.* A33, 426–429.
SCHERINGER, C. (1977*c*). *Acta Cryst.* A33, 430–433.
SMITH, H. W. & LIPSCOMB, W. N. (1965). PhD Thesis, Havard Univ., Cambridge, Mass., USA.
STEWART, R. F. (1970). *J. Chem. Phys.* 53, 205–213.

Acta Cryst. (1978). A34, 625–634

Electron Microscopy Study of Ordering of Potassium Ions in Cubic $KSbO_3$

BY KATSUMICHI YAGI* AND JOHN M. COWLEY

Physics Department, Arizona State University, Tempe, AZ 85281, USA

(*Received* 2 *November* 1977; *accepted* 2 *February* 1978)

Ordered and disordered states of potassium ions in ⟨111⟩ tunnels in the structure of cubic $KSbO_3$ have been studied by high-resolution electron microscopy. *N*-beam calculations for the images of both the ordered and disordered states reproduce well the observed images. The disordered state changes into the ordered state under electron irradiation during the observations. Electron diffraction from the specimens and optical diffraction from the images show diffuse spots due to small domains of the long-range-ordered state, but no other diffuse scattering due to short-range order has been observed.

1. Introduction

Unlike M^+NbO_3 and M^+TaO_3, $KSbO_3$ does not form the cubic perovskite structure (Goodenough & Kafalas, 1973). It generally has the rhombohedral ilmenite structure. However, by annealing at 1000°C, by applying high pressure at 800°C or by synthesis by a flux evaporation technique at about 1000°C in an open Pt crucible (see, for example, Brower, Minor, Parker, Roth & Waring, 1974), a body-centered cubic structure with a parameter of 9·650 Å is stabilized. The structure is composed of SbO_6 octahedra which share edges or corners with each other forming the network shown in Fig. 1. The figure is seen from the [010] direction, where white octahedra are in the $(x,0,z)$ plane and shaded ones are in the $(x,\frac{1}{2},z)$ plane. The structure is characterized by large tunnels along ⟨111⟩, penetrating each other. They meet at the center of the front face in Fig. 1. The K^+ ions are weakly bound in these tunnels and are mobile along them three-dimensionally. The conductivity behavior has been discussed in comparison with the two-dimensional superionic conductor, β-alumina.

Two structures have been reported for $KSbO_3$. One has space group $Pn3$, where K^+ ions are in an ordered state. The other has $Im3$ with K^+ ions in a disordered state. The positions of the K^+ ions are as follows; along a line in a [111] tunnel from the center of the front face in Fig. 1 to one of the body-centered equivalent positions, the line is surrounded by a sequence of four oxygen triangles denoted by O_1, O_2, O_2 and O_1, where the O_1 triangle has oxygens at the corners of edges shared by neighboring octahedra, and the O_2 triangle consists of atoms at corners of corner-sharing octa-

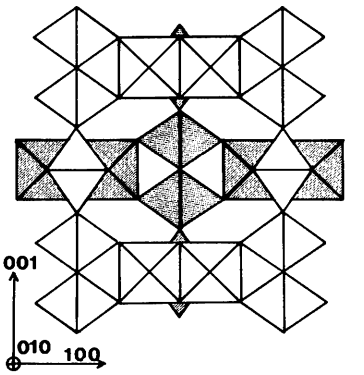

Fig. 1. A [010] projection of the SbO_6 octahedron network in cubic $KSbO_3$. White octahedra, centered on the $(x,0,z)$ plane, form a square arrangement and a large hole. Those shaded are on the $(x,\frac{1}{2},z)$ plane.

* Present address: Physics Department, Tokyo Institute of Technology, Oh-okayama, Meguro-ku, Tokyo 152, Japan.